Di-Vector Boson and a Jet Production via Gluon-Gluon Fusion

Pankaj Agrawal
Institute of Physics
Bhubaneswar, India

in collaboration with

Ambresh Shivaji
(HRI, Allahabad)

September 24, 2013

Outline

Introduction

Processes

Calculation and Checks

Numerical Results

Conclusion

Introduction

- LHC has now completed the run I. The standard model is in excellent agreement with the collected data.
- Simplest extensions and modifications of the standard model are getting seriously constrained.
- The Higgs mechanism of the standard model now seems to have been validated with the discovery of a Higgs boson like neutral scalar particle. The strong evidence has been presented by the both CMS and ATLAS Collaborations. Because of the appearance of the signal in multiple channels, there is little doubt that the Higgs boson of the standard model has been found.
- It would appear that to look for the directions for the extension, one may need to probe as many standard model processes as possible.
- In particular, one may wish to look for processes that have many particles in the final state, or have small cross-sections.

Introduction

- At LHC and proposed hadron colliders such as HE-LHC, one of the features is large gluon luminosity.
- This has already been seen for a number of processes. The processes with one or two gluons become more important as one goes from Tevatron energies to LHC energies and beyond.
- Therefore, processes with gluon-gluon scattering would be important and observable at LHC/HE-LHC.
- Such processes can also contribute to the backgrounds to the beyond-the-standard-model physics scenarios.
- We are interested in a particular set of processes $pp \to VV'g/\gamma X$. Here $V, V' = W, Z, \gamma$. We are particularly interested in the contribution from the gluon-gluon scattering. Since W, Z, γ do not couple to the gluons directly, these processes take place at the one-loop.

Introduction

- The results for the $gg \to \gamma\gamma g$ have been available for more than 10 years. This process contributes to the observed process $pp \to \gamma\gamma j$.
- In this conference, the results have been presented for QCD corrections at NLO to $pp \to \gamma\gamma j$.
- By the counting in α_s, gluon-gluon annihilation, though a one-loop process, contributes at NNLO order.
- Preliminary results for $gg \to \gamma Z g$ were presented in the last RADCOR (2011) by Ambresh. Since then, many groups have computed such processes.
- We will be presenting our results for the following processes:

$$\begin{aligned} gg &\to \gamma Z g, \gamma\gamma g, \gamma Z \gamma \\ gg &\to ZZg \\ gg &\to WWg \end{aligned}$$

Introduction

- After presenting results for these processes, we shall be looking at the process $gg \rightarrow \gamma Zg$ in some detail. This presentation is based on *P. A. and A. Shivaji, Phys Rev D (2012) and JHEP (2013)*.

Outline

Introduction

Processes

Calculation and Checks

Numerical Results

Conclusion

Processes

- These processes take place at one-loop. There is no contribution at the tree level. This is because we have electroweak bosons in the processes with no external quarks. Therefore, one-loop order is the leading order.
- The one loop diagrams that make contribution are box-type and pentagon-type diagrams. For the processes involving W-bosons, there are also triangle diagrams.
- These diagrams have a quark loop. We have taken the first five flavours to be massless. The top quark contribution has also been included.
- It turns out triangle diagrams don't contribute and last set of diagrams give small contribution So we have included only first two type of diagrams.
- For each quark flavour, we have 24 pentagon-type and 18 box-type diagrams. Only half of these diagrams are independent.

Processes

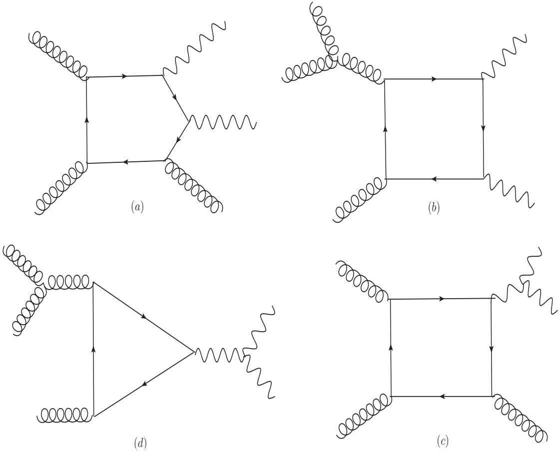

Fig 1: Typical diagrams contributing to the processes.

Processes

- For the $gg \to \gamma Zg, WWg, ZZg$ processes, the amplitude can be written as:

$$\begin{aligned}
\mathcal{M}^{abc}(gg \to VV'g) &= i\frac{f^{abc}}{2}\mathcal{M}_V(VV'g) + \frac{d^{abc}}{2}\mathcal{M}_A(VV'g), \\
\mathcal{M}_V(VV'g) &= -\, e^2 g_s^3\, C_V(VV'g)\ (\mathcal{P}_V - \mathcal{B}_V)\,, \\
\mathcal{M}_A(VV'g) &= -\, e^2 g_s^3\, C_A(VV'g)\ (\mathcal{P}_A)\,.
\end{aligned}$$

- Because of the colour structure, there is no interference between the vector and axial vector part of the amplitude.

Processes

- The various couplings are:

$$
\begin{aligned}
C_V(\gamma Zg) &= \frac{1}{sin\theta_W cos\theta_W}\left(\frac{7}{12}-\frac{11}{9}sin^2\theta_W\right), \\
C_A(\gamma Zg) &= \frac{1}{sin\theta_W cos\theta_W}\left(-\frac{7}{12}\right), \\
C_V(ZZg) &= \frac{1}{sin^2\theta_W cos^2\theta_W}\left(\frac{5}{8}-\frac{7}{6}sin^2\theta_W+\frac{11}{9}sin^4\theta_W\right), \\
C_A(ZZg) &= \frac{1}{sin^2\theta_W cos^2\theta_W}\left(-\frac{5}{8}+\frac{7}{6}sin^2\theta_W\right), \\
C_V(WWg) &= \frac{1}{sin^2\theta_W}\left(\frac{1}{2}\right), \\
C_A(WWg) &= \frac{1}{sin^2\theta_W}\left(-\frac{1}{2}\right).
\end{aligned}
$$

Processes

- If we look at the processes $gg \to \gamma\gamma g, \gamma Z\gamma$, the amplitude can be written as

$$\mathcal{M}^{abc}(gg \to \gamma\gamma g) = i\,\frac{f^{abc}}{2}\,\mathcal{M}_V,$$
$$\mathcal{M}_V = \mathcal{A}_P^V - \mathcal{A}_B^V = -e^2 g_s^3 \left[\left(\frac{11}{9}\right)\mathcal{M}_V^{(0)} + \left(\frac{4}{9}\right)\mathcal{M}_V^{(t)}\right].$$

$$\mathcal{M}^{ab}(gg \to \gamma\gamma Z) = \frac{\delta^{ab}}{2}\,\mathcal{M}_A,$$
$$\mathcal{M}_A = \mathcal{A}_P^A = \frac{e^3 g_s^2}{\sin\theta_W \cos\theta_W}\left[\left(\frac{5}{36}\right)\mathcal{M}_A^{(0)} + \left(\frac{1}{9}\right)\mathcal{M}_A^{(t)}\right].$$

- The process $gg \to \gamma\gamma g$ gets contribution from both pentagon and box type diagrams and is obviously pure vector type.
- For the process $gg \to \gamma Z\gamma$, only pentagon-type diagrams contributes from axial-vector couping of the Z-boson.

Outline

Introduction

Processes

Calculation and Checks

Numerical Results

Conclusion

Calculation

Our calculation proceeds as follows:

- We use traditional Feynman diagram based approach.
- For each class of diagrams, we write down the amplitude for a prototype diagram using the standard model Feynman rules. The amplitude for the rest of diagrams is generated by appropriate permutations of the external legs.
- The trace of γ matrices is computed in *d* dimensions using FORM. The amplitude is now written in terms of tensor integrals.
- This is a brute-force evaluation of the amplitude, so the expression is quite huge. It is to be evaluated numerically.

Calculation

- The most complicated tensor integrals that appear in the calculations are:

$$E^{\mu\nu\rho\sigma\delta} = \int \frac{d^d k}{(2\pi)^d} \frac{k^\mu k^\nu k^\rho k^\sigma k^\delta}{N_0 N_1 N_2 N_3 N_4} , \tag{1}$$

$$D^{\mu\nu\rho\sigma} = \int \frac{d^d k}{(2\pi)^d} \frac{k^\mu k^\nu k^\rho k^\sigma}{N_0 N_1 N_2 N_3} . \tag{2}$$

  Here, $N_i = k_i^2 - m_q^2 + i\epsilon$ and k_i is the momentum of the i^{th} internal line in the corresponding scalar integrals; $d = (4 - 2\epsilon)$ and m_q is the mass of the quark in the loop.
- We also examine the effect of non-zero m_q, e.g., when $q = t$.

Calculation

- For the reduction of the tensor integrals, we have developed a set of routines “OVR”. The reduction has been done using the methods of Oldenborgh and Vermaseren (*Z. Phys. (1990)*).
- OVR can do the reduction up to 5-tensor pentagon integrals. It was first developed for the process $gg \to \gamma\gamma g$ (*P. A. and G. Ladinsky, Phys Rev D (2001)*).
- For massless quarks in the loop, we have computed the scalar integrals. These are used to make certain checks on our calculation.
- For the massive quarks in the loop, we use OneLOop library for the bubble, triangle, and box scalar integrals (*A. van Hameren, Comp. Phys. Comm.(2011)*).
- For the pentagon scalar integrals, we use the result of van Neerven and Vermaseren (*Phys. Lett. (1984)*). Using this technique, one can write a pentagon scalar integral in terms of box scalar integrals.

Checks

We have made a number of checks on our calculation. These are listed below.

- *UV Finiteness*
  The process is expected to be UV finite. Pentagon diagrams are obviously UV finite. But individual box diagram is not. However, when we add box diagrams, the UV divergences cancel. We have checked numerically that the amplitude is UV finite.
- *IR Finiteness*
  The process has mass singularities due to small light quark mass. These singularities show up as $\log^2(\mathrm{m_q})$ and $\log(\mathrm{m_q})$. These large logarithms must cancel. We have checked this cancellation for both types of mass singularities. There is no soft IR divergence, as we will be making p_T cuts on the jets.

Checks

- *Gauge Invariance*
  We also expect gauge invariance with respect to the gauge particles. To check this, we replace the polarization vector of $g/\gamma/Z$ bosons with the corresponding momentum vector. We find that the amplitude vanishes when we make this replacement for the photon, gluon and suitably for the Z-boson.
  For the process $gg \rightarrow VV'g$, the axial part of the amplitude does not interfere with the vector part of the amplitude due to the color factor structure. This factor is symmetric for the axial vector part of the amplitude, while it is antisymmetric for the vector part. We have checked that these parts are separately gauge invariant.

Outline

Introduction

Processes

Calculation and Checks

Numerical Results

Conclusion

Numerical Results

- As we discussed we have made numerous checks to confirm the reliability of our numerical results.
- We compute the amplitude numerically using the real polarization basis for the vector bosons.
- Because of the complexity of the amplitude, the number of diagrams and polarization combinations, it may take about a second to compute the squared amplitude for a phase space point. So we use a PVM implementation of the VEGAS algorithm (AMCI) to do the integration and use a cluster of machines to get the numerical results (*S. Veseli, Comp. Phys. Comm.(1998)*).
- It takes about 8-10 hours on about 30 cores of a Xeon based computing system to get the results.

Numerical Results

- In Fig 2, we display the cross sections as a function of CM energy. These results include following kinematic cuts:

$$P_T^{\gamma,W,Z,j} > 30\ \mathrm{GeV},\ |\eta^{\gamma,\mathrm{Z,j}}| < 2.5,\ \mathrm{R}(\gamma,\mathrm{j}) > 0.6.$$

  We have also chosen factorization and renormalization scales as $\mu_f = \mu_R = E_T^{\gamma,Z,W}$. PDFs are CTEQ6M.
- For the CM energy of 8 TeV, the cross sections are about 47, 95 and 225 fb for $\gamma Zg, ZZg, WWg$ processes respectively. Clearly, thousands of such events have already been produced at the LHC. For CM energy of 14 TeV, these numbers are about a factor of 3 larger.
- For a comparison, we have also plotted the cross sections for the $gg \to \gamma Z, ZZ, WW$. We see that both sets of processes have similar behaviour.

Numerical Results

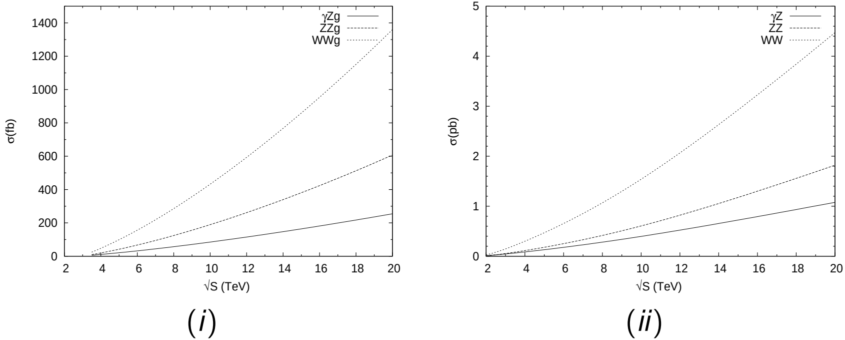

Fig 2: Centre of mass energy dependence of the cross sections of the processes (i) $VV'g$ (ii) VV'.

Numerical Results

- Cross sections for the $\gamma Zg, ZZg, WWg$ processes are about $20 - 30\%$ of the corresponding $gg \to \gamma Z, ZZ, WW$ processes for 14 TeV CM energy.
- A second comparison can be made with LO $pp \to \gamma Zj, ZZj, WWj$ processes. Here, we find that cross sections for the $gg \to \gamma Zg, WWg$ are about $4 - 5\%$ of the LO corresponding processes, but for $gg \to ZZg$ it can be $10 - 15\%$ of the corresponding tree level process.
- Interesting this percentage is similar for $gg \to \gamma Z, ZZ, WW$ processes.
- Cross sections for the tree level processes were generated using MadGraph.
- NLO QCD corrections to the $pp \to \gamma Zj, ZZj, WWj$ are also being done by many groups. *T. Melia et al, JHEP (2012)* has a detailed study of the $gg \to WWg$ process. Next, we will look at the $gg \to \gamma Zg$ a bit more closely.

Numerical Results

- In our calculations for γZg process, we have also considered the diagrams with a top quark in the loop. We find that the top-quark makes negligible contribution to the process. From Fig 3, it appears that this decoupling of a quark occurs starting around $m_q = 100 GeV$. Because of the similar nature of the processes under consideration, we can neglect diagrams with a top quark in the loop.
- For the process, AV and V contributions are separately gauge invariant. From Fig 4, we see that AV contribution is quite small – only about 10%. AV contribution is only from pentagon diagrams. We also see that bulk of the contribution is from box diagrams.
- In Fig 5(ii), we show the μ dependence by varying it by a factor of 2. We see that the cross section can increase by about 40%, or decrease by about 25%. This large dependence is not surprising, as the process is effectively a LO process.

Numerical Results

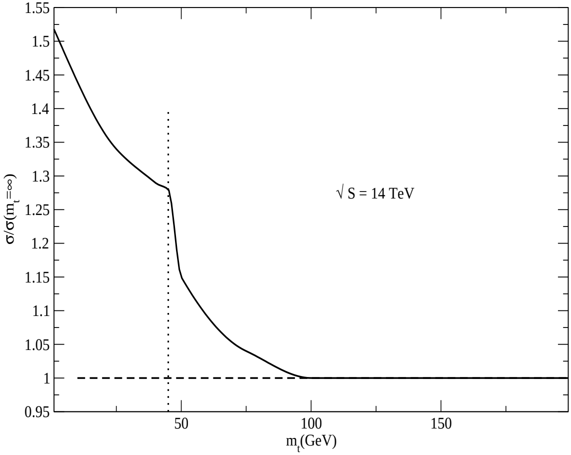

Fig 3: Decoupling of the top quark in the process $gg \to Z\gamma g$.

Numerical Results

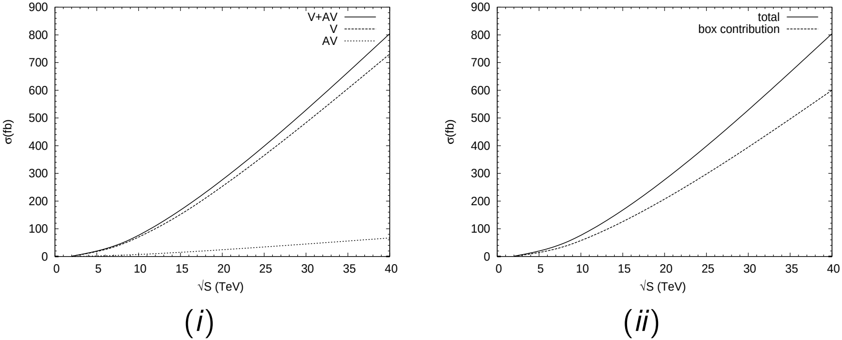

Fig 4: Contributions to $Z\gamma g$ production (i) V and AV (ii) Box and Pentagon.

Numerical Results

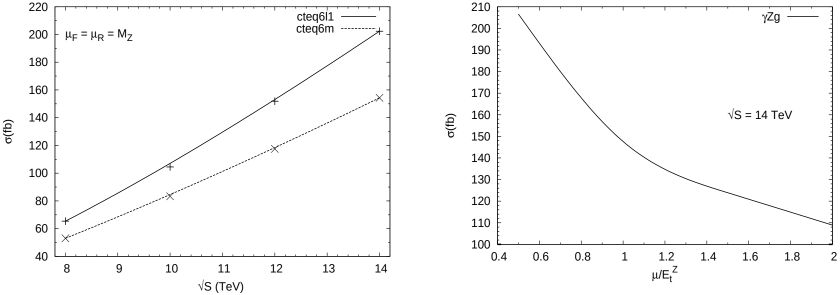

(*i*) (*ii*)

Fig 5: For $Z\gamma g$ production (i) PDF and (ii) μ dependence.

Numerical Results

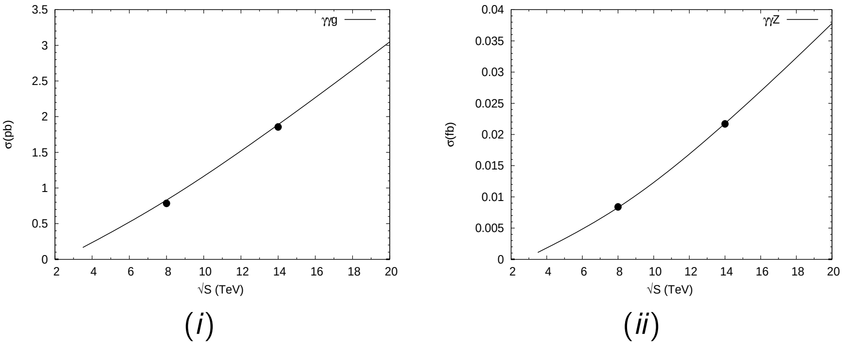

Fig 6: Cross sections for the production of (i) $\gamma\gamma g$ and (ii) $\gamma\gamma Z$.

Numerical Results

- The results for the process $gg \to \gamma\gamma g$ are already in literature for massless quark in the loop. We included heavy-quark, top-quark, in the calculation and found that it made negligible contribution. The typical cross-section for, at 14 TeV LHC, is about 2 pb.
- The cross-section for the process $gg \to \gamma\gamma Z$ is quite small, as expected. It is about 0.02 fb for 14 TeV CM energy. So without, high-luminosity option at the LHC, this process would not be observable.

Numerical Results

$\sqrt{S}$ (TeV)	$p_T^{\gamma,min}$ (GeV)	$\sigma^{\rm LO}$ (pb)	$\sigma^{\rm NLO}$ (pb)	$\sigma_{gg}^{\rm NNLO}$ (fb)	r (%)
8	30	2.2	3.4	46.1	3.8
	50	1.1	1.7	30.5	5.1
14	30	4.9	7.7	158.7	5.7
	50	2.6	4.2	109.9	6.0
35	30	14.9	23.5	854.1	9.9
	50	8.2	13.5	607.3	11.5

Numerical Results

- In the table r represents the NNLO correction as a fraction of NLO correction (i.e. $\sigma_{gg}^{\rm NNLO}/(\sigma^{\rm NLO} - \sigma^{\rm LO})(\%)$.
- For the Fig 5(i) and the table we have used the cuts:

$$p_T^j > 30 \text{ GeV}, \ p_T^\gamma > 15 \text{ GeV}, \ p_T^l > 10 \text{ GeV}, \ |\eta^{\gamma,l,j}| < 2.5,$$

$$R(\gamma,j), R(l,\gamma), R(l,j), R(l,l) > 0.4.$$

- Here l represents a lepton in which a Z-boson decays.
- In the table, we have LO and NLO results to compare with our results. These LO and NLO results were generated using the MCFM code.
- As one would expect, the NNLO correction increases as one goes to higher center-of-mass energy, or higher p_T on the photon.
- As the cross sections are only small fraction of LO, or NLO, it will be a challenge to observe the mechanism.

Outline

Introduction

Processes

Calculation and Checks

Numerical Results

Conclusion

Conclusion

- We have presented the results for the processes $gg \to \gamma Zg, WWg, ZZg, \gamma\gamma g, \gamma Z\gamma$. These processes occur at one loop through pentagon and box-type diagrams.
- We have used a set of reduction routines, OVR, based on the Oldenborgh-Vermaseren scheme. Cross sections are only a few percent of LO, or NLO contributions.
- We find that there is decoupling of the top-quark. So its contribution is negligible.
- These are standard model processes and cross-sections are large enough so that there are already thousands of such events at the LHC. But, it may take some effort to make sure that such processes have occurred at the LHC.